Rare Met. (2019) 38(5):420–427
https://doi.org/10.1007/s12598-019-01253-y

RARE METALS
www.editorialmanager.com/rmet

Synthesis of TiO_2@$ZnIn_2S_4$ hollow nanospheres with enhanced photocatalytic hydrogen evolution

He Li, Zi-Hao Chen, Lei Zhao, Gui-Dong Yang*

Received: 29 December 2018 / Revised: 16 January 2019 / Accepted: 15 March 2019 / Published online: 6 April 2019

Abstract In this work, we designed and prepared the novel TiO_2@$ZnIn_2S_4$ nano-sized hollow structure via templating method assisted by hydrothermal synthesis process. Its unique hollow structure and type-II heterojunction between TiO_2 hollow nanospheres and $ZnIn_2S_4$ nanosheet can provide enough interior cavities and transfer paths for the light absorption and charge quick migration. The crystal structure, morphology and charges separation property were measured. The characterization results show that the hollow-structured TiO_2@$ZnIn_2S_4$ was successfully prepared, and the optimal sample exhibited excellent photocatalytic hydrogen generation compared with TiO_2/$ZnIn_2S_4$ cluster exceeding by a factor of 1.1 under overall light irradiation. Specially, the detailed mechanism of the photocatalytic H_2 evolution and charge carrier migration for the as-prepared TiO_2@$ZnIn_2S_4$ hollow nanosphere was also studied.

Keywords TiO_2; $ZnIn_2S_4$; Photocatalysis; Hydrogen evolution; Hollow

1 Introduction

The mitigation energy crisis has attracted numerous research interests in the field of green energy and renewable sources in recent years [1–3]. Photocatalytic hydrogen generation can be regarded as a promising way to solve this dilemma due to its renewability, stabilization and cleanliness. In particular, the hollow nanostructured materials are viewing a novel model because it can enhance the light absorption, reagent enrichment and efficient interfacial reaction during the photoinduced hydrogen evolution reaction (HER). Therefore, the nano-sized hollow structure and its derivative nanomaterials such as core–shell, yolk–shell and ball-in-ball-structured semiconductor materials have been applied in energy storage, catalysis and electrochemistry [4–6]. Among the above multilevel structure, the classical core–shell hollow structure has the follow advantages. Firstly, when the light was penetrated into the nano-sized hollow structure, it would trigger the multiple scattering effect because the photon could be scattered by the inner shell and the pore structure for the enhanced utilization of proton energy compared with other morphology of photocatalysts. Secondly, the hollow structure would provide a relative homogeneous reaction space for boosting the HER activity. Finally, the hollow structure could offer the larger specific surface area and pore structure could increase the mass transfer efficiency or active sites during the H_2 evolution [4]. Hence, it is highly expected to establish a novel core–shell hollow nanostructured material for effective photocatalytic H_2 generation.

Titanium dioxide (TiO_2) with the formidable defect of low light utilization and relative wide band gap (3.20 eV) greatly limited its practical application. Hence, a plenty of efforts are paid to improve its performance, including the lattice-doping, morphological control and heterogeneous structure construction. In term of the above research, Wang et al. [7] have reported the growth of $ZnFe_2O_4$ nanoparticles on TiO_2 nanotube arrays for enhanced visible-light

H. Li, Z.-H. Chen, G.-D. Yang*
XJTU-Oxford International Joint Laboratory for Catalysis, School of Chemical Engineering and Technology, Xi'an Jiaotong University, Xi'an 710049, China
e-mail: guidongyang@xjtu.edu.cn

L. Zhao
School of Civil Engineering and Architecture, Xinxiang University, Xinxiang 453003, China

photocatalytic activity. Xiang et al. [8] have prepared the graphene-modified titania nanosheets for enhanced photocatalytic H_2 production activity. Yang et al. [9] have reported the novel three-dimensionally ordered macroporous Fe^{3+}-doped TiO_2 photocatalysts for H_2 production and degradation applications. Nevertheless, due to the relatively low charge transfer efficiency, the above photocatalysts still cannot satisfy the practical application requirement. Therefore, it is desired to synthesize the hollow-structured TiO_2 via anchoring with ternary chalcogenide to form heterojunction and thus enhance the charge separation and migration under overall light irradiation. $ZnIn_2S_4$ as a typical photocatalyst has been widely concerned due to its great optical, electrical properties, suitable band gap (1.99 eV) and promising stability [10]. Therefore, the construction of TiO_2@$ZnIn_2S_4$ core–shell hollow nanospheres could highly improve the transfer efficiency of charge carriers in the heterojunction system. Simultaneously, multiple scattering effect depended on hollow nanostructure could boost the light absorption of catalyst, as a result of leading to high HER activity.

Herein, according to the above theoretical analysis, in this work, we report the formation of TiO_2@$ZnIn_2S_4$ hollow nanospheres which exhibit a great photocatalytic hydrogen evolution under overall light irradiation. This work is expected to pave a way to synthesize the novel hollow core–shell structure, and the detailed mechanism is proposed to explain the migration of photoinduced electrons and holes in this system.

2 Experimental

2.1 Chemical and materials

All chemical reagents were of analytical grade and used without any further purification, including tetraethyl orthosilicate (TEOS, $\geq$ 99.5%), tetrabutyl titanate (TBOT, $\geq$ 98%), potassium chloride (KCl, $\geq$ 99.5%), indium nitrate ($In(NO_3)_3$, $\geq$ 99.99%), zinc nitrate hexahydrate ($Zn(NO_3)_2{\cdot}6H_2O$, 99.998%), thioacetamide (TAA, 98%), 2-propanol (C_3H_8O, $\geq$ 99.5%), methyl alcohol (CH_3OH, 99%), ammonium hydroxide ($NH_3{\cdot}H_2O$, $\geq$ 99.5%), sodium hydroxide (NaOH, 99%).

2.2 Synthesis of SiO_2 nanospheres

The monodisperse SiO_2 template was synthesized by the Stöber method. Briefly, 40 ml 2-propanol, 1.5 ml ammonia solution and 2.0 ml deionized water were mixed and stirred vigorously in a flask. And then, 3.5 ml TEOS was added rapidly and stirred for 24 h at room temperature. Afterward, the predecessor was collected by the centrifugation and washed several times with deionized water and dried in a 60 °C oven for 5 h.

2.3 Preparation of TiO_2 hollow nanospheres

The synthesis of TiO_2 hollow nanospheres was prepared by the following method. First, 40 ml methyl alcohol and 0.3 ml potassium chloride solution (0.1 mol·L^{-1}) were ultrasonically dissolved and added 0.1 g SiO_2 nanospheres in a reaction vessel. Then, 0.5 ml TBOT was added rapidly and stirred for 4 h at room temperature. The samples were washed several times with ethyl alcohol and dried in a 60 °C oven for 5 h and then calcined at 500 °C for 1 h in a muffle furnace. After the products were cooled down to room temperature, NaOH aqueous solution (10 mol·L^{-1}) was added into the solution to etch SiO_2 template and the products were washed with deionized water and dried in a 60 °C oven for 5 h.

2.4 Preparation of TiO_2@$ZnIn_2S_4$ hollow nanospheres

The TiO_2@$ZnIn_2S_4$ hollow nanospheres were prepared by the hydrothermal method. The optimal procedures were described as follows: 0.5 mmol cadmium chloride, 1.0 mmol thiourea and 4.0 mmol thioacetamide were dissolved in a flask containing 40 ml deionized water. Afterward, the certain amount of TiO_2 hollow nanospheres was added into the above mixture and stirred for 4 h. Then, the solution was transferred to a 100-ml Teflon-lined stainless steel autoclave which was heated to 180 °C for 3 h, it was then cooled to room temperature and washed with deionized water and ethanol several times. Afterward, the samples were dried in a 60 °C oven for 5 h.

2.5 Preparation of TiO_2/$ZnIn_2S_4$ composite

The synthesis of TiO_2 cluster was carried out by the following method. Typically, 30.0 ml methyl alcohol and 0.5 ml deionized water were mixed in a reaction vessel. Then, 1.0 ml TBOT was added rapidly and vigorously stirred for 4 h at room temperature. Afterward, the predecessor was washed several times with deionized water, dried in a 60 °C oven for 4 h and then calcined at 500 °C for 1 h in a muffle furnace. After the products were cooled down to room temperature, 0.5 mmol cadmium chloride, 1.0 mmol thiourea and 4.0 mmol thioacetamide were dissolved in a flask containing 40 ml deionized water stirring for 4 h. Then, the following process was the same with the preparation of TiO_2/$ZnIn_2S_4$ nanospheres.

2.6 Characterization

The experimental samples were tested by various measurements. The crystal phase of as-prepared samples was analyzed using X-ray diffractometer (XRD, Lab X XRD-6100, SHIMADZU). The structure and morphology of the products were investigated using a field emission scanning electron microscope (FESEM, JSM-6700F, JEOL) equipped with an energy-dispersive spectrometer (EDS) and transmission electron microscope (TEM, JEM-2100, JEOL). The ultraviolet–visible (UV–Vis) spectra over the samples were obtained by a UV–Vis spectrophotometer (UV-2600, SHIMASZU). The electrochemical measurements were obtained to test on a CHI660E electrochemical apparatus (Shanghai, China) using a standard three-electrode cell equipped a working electrode, a platinum wire and Ag/AgCl as the counter electrode and reference electrode, respectively. The electrolyte was 1.0 mol·L^{-1} Na_2SO_4 solution. The surface photovoltaic spectrum (SPS) was carried out using a solid junction cell with a light source-monochromator-lock-in detection apparatus. Then, the samples were irradiated by the 500-W xenon lamp with a triple-prism monochromator (Hilger and Watt, D300). And an amplifier (Brookdeal, 9503-SC) was synchronized with a light chopper, which was obtained to amplify the signal of photovoltage. The SPS signals were normalized to unity at the characteristic peaks, which were measured by a laptop, respectively. All the SPS measurements were performed at room temperature.

2.7 Photocatalytic H_2 evolution

The photocatalytic water splitting reaction was analyzed in a Pyrex reactor for photoinduced irradiation at room temperature. Typically, 0.03 g sample was dispersed in 40 ml aqueous solutions that contain 5 ml lactic acid (sacrificial electron donor). And the reaction vessel was deaerated by the bubble treatment using the high purity nitrogen. Then, the evolved gases were evaluated by an online gas chromatography (SP-2100A, Beifen-Ruili) with the thermal conductivity detector (TCD) detector and the photocatalytic reaction was tested under the irradiation of a 300-W xenon lamp (HSX-F300, Nbet Beijing).

The recycled experiments of photocatalytic reactions were analyzed under the above conditions to test the sustainable property. After 4-h photocatalytic H_2 evolution reaction, the suspensions were washed and centrifuged by ethanol several times and then dried in an oven for 3 h at 50 °C. The drying photocatalyst was re-dispersed in 40 ml deionized water with 5 ml lactic acid in reaction vessel, respectively. Before the photoreaction, the system was degassed to remove the air in the reaction solution.

The apparent quantum yield (AQY) of photocatalytic H_2 production was tested on the similar condition. A xenon lamp with different monochromatic lights was as the light source (λ = 435 nm). The illuminated area on the reaction cell was about 4.52 cm^2. The average photocatalytic H_2 generation rate was measured after 3 h. Afterward, the AQY for H_2 evolution was calculated according to the following equation [4]:

$$\mathrm{AQY} = \frac{N_{\mathrm{re}}}{N_{\mathrm{ip}}} \times 100\% = \frac{2N_{\mathrm{ehm}}}{N_{\mathrm{ip}}} \times 100\% \quad (1)$$

where N_{re} is the number of reactor electrons, N_{ip} is the number of incident photons and N_{ehm} is the number of evolved hydrogen molecules.

3 Result and discussion

The overall synthetic process of TiO_2@$ZnIn_2S_4$ hollow nanospheres is shown in Fig. 1. Firstly, monodisperse SiO_2 nanospheres were prepared by a previously reported Stöber method with modification [4]. And then, the solvent–thermal method was adopted to synthesize SiO_2@TiO_2 core–shell composite. Afterward, the resulted white powder underwent ultrasonic exfoliation to obtain homogeneous solution, while the selective etching of SiO_2 inner core was used to obtain the TiO_2 hollow nanospheres. Then, the precursors of metal ions Zn^{2+} and In^{3+} can be preloaded onto the surface of TiO_2 hollow nanospheres owing to their electrostatic interaction. Next, under the hydrothermal reduction process, the thioacetamide acted as a sulfur source would react with Zn^{2+} and In^{3+} to in situ generate and anchor $ZnIn_2S_4$ nanoleaves on the surface of TiO_2 nanospheres, which finally leads to the formation of TiO_2@$ZnIn_2S_4$ hollow heterojunction.

The crystal phase of the as-synthesized composites was measured by XRD. As shown in Fig. 2a, the main characteristic peaks at 25.2°, 38.5°, 48.0°, 55.0° and 62.6° in

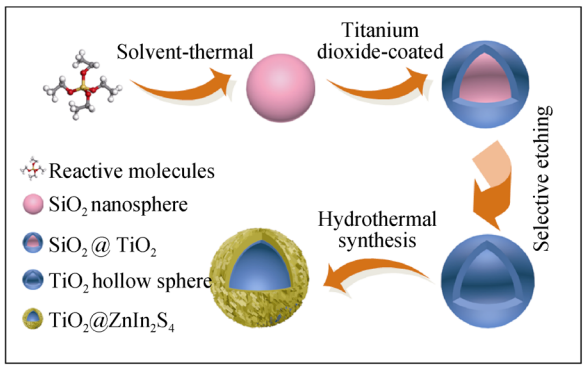

Fig. 1 Schematic representative of formation procedure for as-synthesized TiO_2@$ZnIn_2S_4$ hollow nanospheres

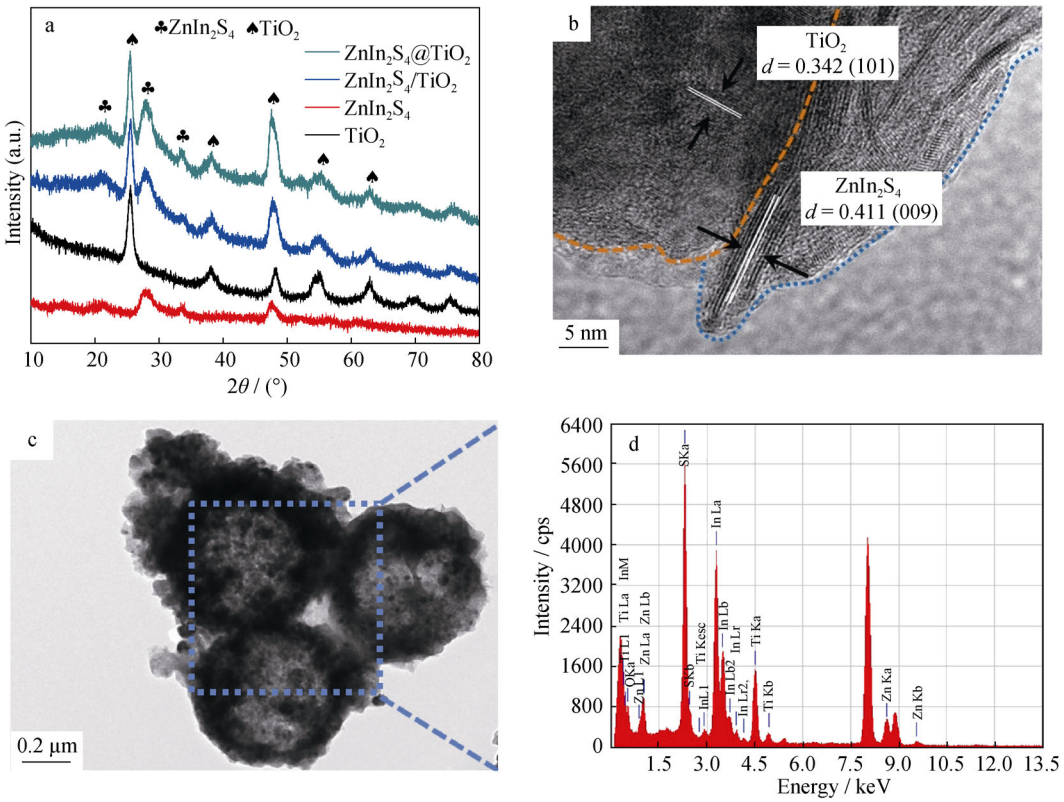

Fig. 2 XRD patterns of **a** as-synthesized samples and **b** HRTEM image of optimal sample (TiO_2@$ZnIn_2S_4$ hollow nanospheres); **c** TEM image and **d** EDS result of optimal sample

the curve of the pure TiO_2 can be, respectively, assigned to the (101), (004), (200), (211) and (204) diffraction plane of the anatase structure TiO_2 (JCPDS No. 21-1272). And the three main characteristic peaks located at 21.5°, 28.3° and 54.8° correspond to the (009), (104) and (021) diffraction plane of the rhombohedral structure $ZnIn_2S_4$ (JCPDS No. 49-1562), respectively [11, 12]. Specially, Fig. 2b shows the typical high-resolution TEM (HRTEM) of the TiO_2@$ZnIn_2S_4$ hollow nanospheres, which can be matched to the lattice fringes of 0.342 and 0.411 nm, corresponding to the (101) crystal plane of anatase TiO_2 and the (009) crystal plane of rhombohedral $ZnIn_2S_4$, respectively. In addition, the corresponding EDS data are displayed in Fig. 2c, d, and the titanium (Ti), oxygen (O), zinc (Zn), indium (In) and sulfur (S) elements can be observed. These above results demonstrate that $ZnIn_2S_4$ nanoleaves are uniformly anchored on the surface of TiO_2 hollow nanospheres and strongly support that the novel TiO_2@$ZnIn_2S_4$ hollow nanospheres are successfully obtained.

Figure 3a–d show the SEM images of the as-prepared samples. It can be seen that the SiO_2 template exhibits the typically spherical morphology with the average diameter of 450 nm in Fig. 3a. And the pure TiO_2 hollow nanosphere has an obvious inner cavity with the average of diameter of 720 nm in Fig. 3b. The pure $ZnIn_2S_4$ exhibits the micron-sized flower-like structure with the average diameter of 4 μm. Figure 3d shows the SEM image of the TiO_2/$ZnIn_2S_4$ cluster sample. As shown, a typical irregular TiO_2 agglomerates and the flower-like $ZnIn_2S_4$ nanoleaves are uniformly dispersed on the surface of TiO_2 cluster. Figure 3e, f clearly show the TEM images of TiO_2@$ZnIn_2S_4$ hollow nanospheres. The as-obtained sample possesses typical spatial cavity with the average diameter of 520 nm and outer shell with about 100 nm in thickness, which is beneficial for the light absorption and reactant enrichment in their inner cavity, leading to the great enhancement of the photocatalytic H_2 generation [13].

The time-dependent water splitting over the as-prepared samples were tested under overall light irradiation. As shown in Fig. 4a, the pure TiO_2 and $ZnIn_2S_4$ cluster displays lower photocatalytic H_2 evolution of 205 and 1859 $\mu mol \cdot g^{-1}$ within 4-h photoreaction. Interestingly, the TiO_2/$ZnIn_2S_4$ cluster shows relatively higher H_2 evolution activity of 4518 $\mu mol \cdot g^{-1}$ compared to the pristine samples. Incredibly, the optimal TiO_2@$ZnIn_2S_4$ hollow nanosphere possesses the highest H_2 evolution of 4958 $\mu mol \cdot g^{-1}$, which is 1.1 times higher than the TiO_2/$ZnIn_2S_4$ cluster during the 4-h HER reaction. The photocatalytic recyclability of the optimal sample was measured under the same condition. As shown in Fig. 4b, the optimal

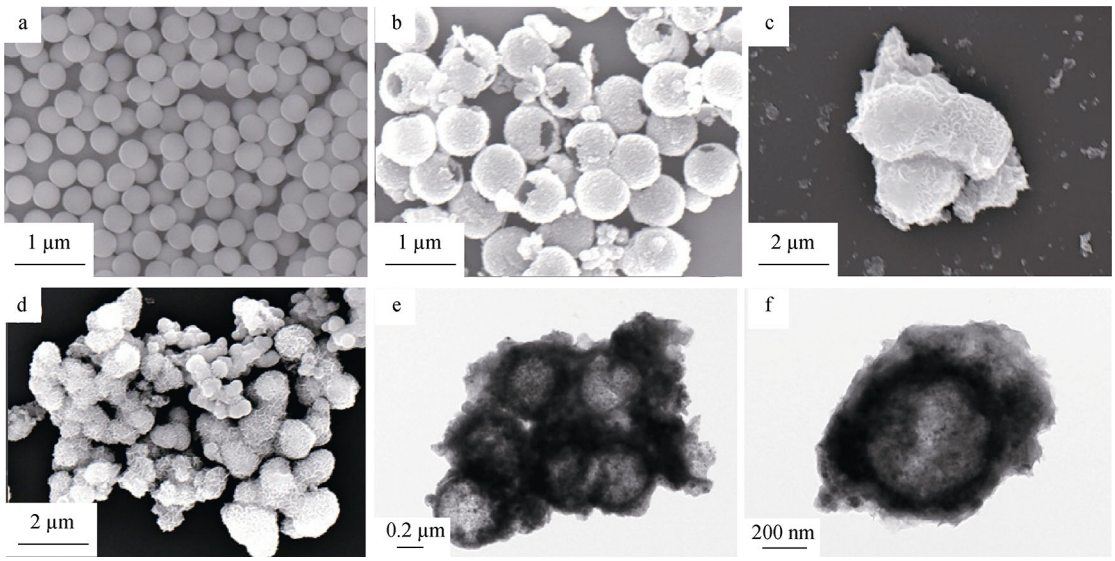

Fig. 3 SEM images of **a** SiO_2 nanospheres **b** TiO_2 hollow nanospheres, **c** pure $ZnIn_2S_4$ cluster and **d** $TiO_2/ZnIn_2S_4$ cluster; **e**, **f** TEM images of optimal sample ($TiO_2@ZnIn_2S_4$ hollow nanospheres)

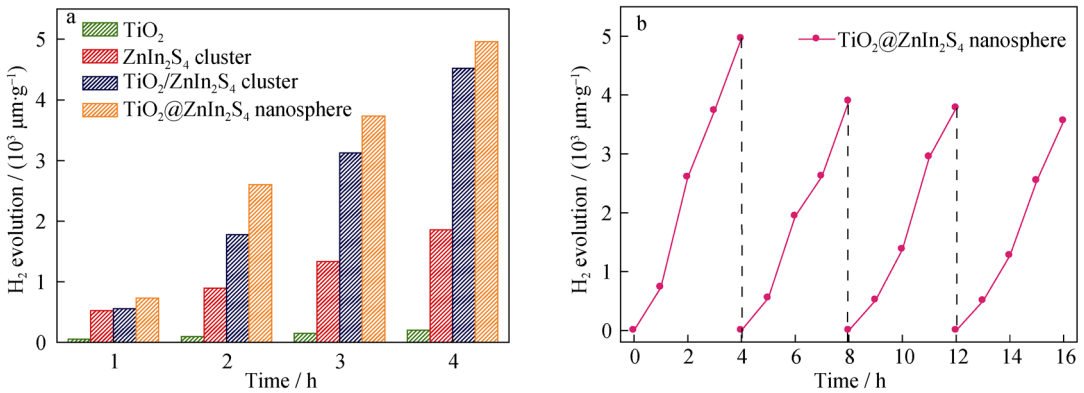

Fig. 4 **a** H_2 evolution for as-synthesized samples under overall light irradiation; **b** cycling runs experiments of photoinduced hydrogen evolution for optimal sample under overall light irradiation

sample maintains a promising HER activity from 4958 to 3560 $\mu mol \cdot g^{-1}$ after 4-cycle photoreaction. The above decline in the photocatalytic H_2 activity may be due to the fact that the catalyst was consumed during the washing and drying process. On the other hand, the core–shell hollow structure has low mechanical strength and is easy to break, leading to the above result. In addition, the apparent quantum yield (AQY) of the $TiO_2@ZnIn_2S_4$ hollow nanosphere was measured at the incident light (435 nm) through the use of band-pass filters under the photocatalytic reaction [14, 15]. The apparent quantum yield of the $TiO_2@ZnIn_2S_4$ hollow nanosphere is 1.84%.

The efficient transfer and separation of charge carriers over the samples (TiO_2 hollow nanosphere, $ZnIn_2S_4$ cluster, $TiO_2/ZnIn_2S_4$ cluster and $TiO_2@ZnIn_2S_4$ hollow nanosphere) were elucidated by transient photocurrent–time measurements. As shown in Fig. 5a, it is clearly observed that the optimal $TiO_2@ZnIn_2S_4$ hollow nanosphere exhibits an apparently stronger photocurrent density compared to the other samples. Additionally, both the $ZnIn_2S_4$ cluster and $TiO_2/ZnIn_2S_4$ cluster display relatively higher photocurrent density in comparison with the pure TiO_2. Figure 5b shows electrochemical impedance spectra (EIS) Nyquist plots of $TiO_2@ZnIn_2S_4$ hollow nanosphere. The impedance is a complex number that can be expressed as the real part and the imaginary part, where the horizontal axis Z' represents the real impedance (Z_{re}) and the vertical axis Z'' is imaginary impedance (Z_{im}). It can be seen that the obtained composite photocatalyst represents the smallest arc radius among these samples, indicating that the nano-sized hollow structure has the lower internal resistance of charge transfer in comparison with the other TiO_2-based nanoclusters.

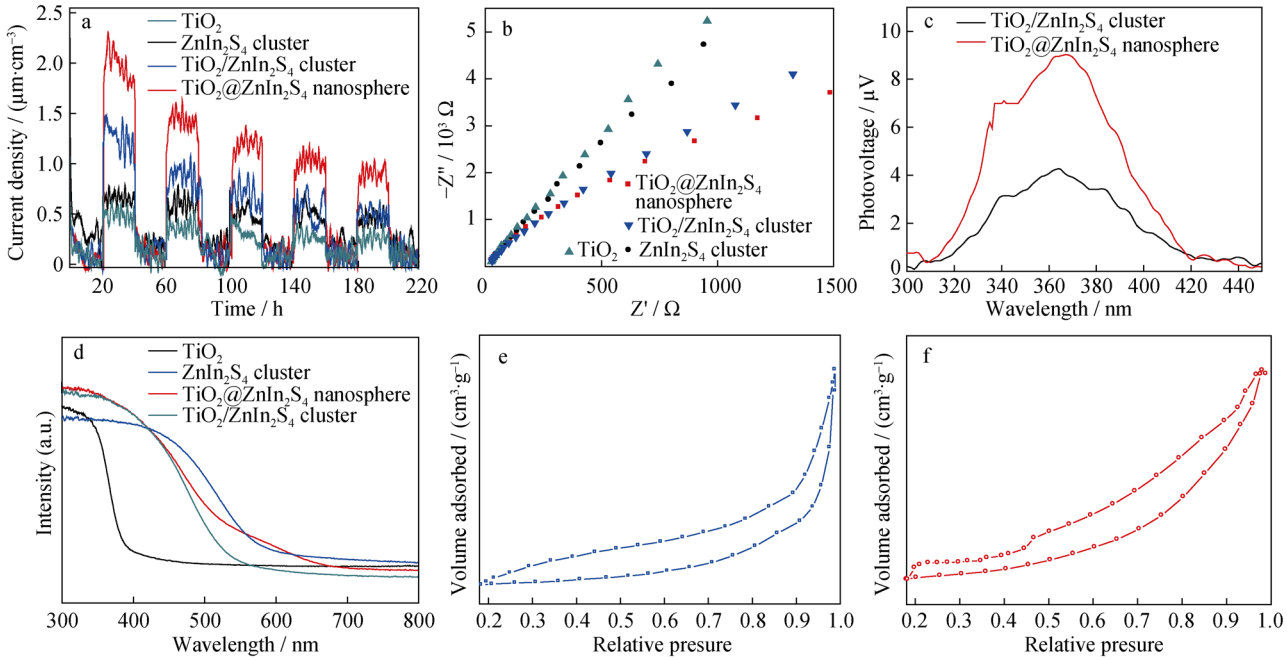

Fig. 5 **a** Transient photocurrent response spectra and **b** EIS Nyquist plots for as-synthesized samples; **c** surface photovoltaic spectrum of and **d** UV–Vis DRS spectra of as-synthesized samples; N_2 adsorption/desorption isotherms of **e** TiO_2/$ZnIn_2S_4$ cluster and **f** TiO_2@$ZnIn_2S_4$ hollow nanosphere

In addition, the SPS was used to further explore the efficiency of photogenerated electrons migration over the samples. To be extended, the stronger the SPS signal is, the easier the charges separation is. Figure 5c reveals that the TiO_2@$ZnIn_2S_4$ hollow nanospheres show much stronger SPS response signal than that of TiO_2/$ZnIn_2S_4$ cluster in the region of 300–450 nm, which clearly confirm the enhanced capability of charges separation, thus ultimately causing the improvement in HER activity. And the data of SPS spectra are consistent with the result of transient photocurrent test.

As shown in Fig. 5d, the optimized TiO_2@$ZnIn_2S_4$ hollow nanosphere has the increased light absorption in the wave region of 300–450 nm among the as-formed samples. This phenomenon can be ascribed to the multiple scattering effect produced by the inner cavity of the hollow nanostructure, which is beneficial for the enhancement of the light absorption. More significantly, the light harvesting of TiO_2/$ZnIn_2S_4$ cluster in the range of 300–450 nm is higher than that of the pure TiO_2 and $ZnIn_2S_4$. And the pure TiO_2 shows the lowest visible-light absorption in the range of 360–600 nm among the as-prepared samples. As evident from these results, it can be concluded that the hollow nanostructure has a positive influence on the optical properties of photocatalyst [16, 17]. As illustrated in Fig. 5e, f, both the TiO_2/$ZnIn_2S_4$ cluster and the optimal TiO_2@$ZnIn_2S_4$ hollow nanosphere sample show the typical type IV isotherm with the H3-type hysteresis loop. The detailed texture properties of the two samples are shown in Table 1, it can be seen that TiO_2/$ZnIn_2S_4$ cluster exhibits low active surface area (11.18 $m^2 \cdot g^{-1}$), and TiO_2@$ZnIn_2S_4$ hollow nanosphere has much larger active surface area (79.72 $m^2 \cdot g^{-1}$), which demonstrates that the nano-sized hollow structure could expose numerous active sites and produce relative larger porous structure for enhancing mass transfer and boosting photocatalytic H_2 evolution reaction.

According to above studies, we attempt to explore the detailed mechanism of charge carrier migration for solar-driven hydrogen generation in the TiO_2@$ZnIn_2S_4$ hollow nanosphere photocatalyst under overall light irradiation. It can be seen in Fig. 6 that due to the accurate positions of valence band (VB) and conduction band (CB) between TiO_2 hollow nanosphere and $ZnIn_2S_4$ cluster, the type-II binary heterojunction can be easily formed. Therefore, when the TiO_2@$ZnIn_2S_4$ sample was irradiated by the solar

Table 1 BET surface area (S_{BET}), average pore size (d) and pore volume (V) of as-prepared samples

Samples	S_{BET}/ ($m^2 \cdot g^{-1}$)	d/ nm	V/ ($cm^3 \cdot g^{-1}$)
TiO_2/$ZnIn_2S_4$ cluster	11.18	2.50	0.097
TiO_2@$ZnIn_2S_4$ hollow nanosphere	79.72	4.95	0.212

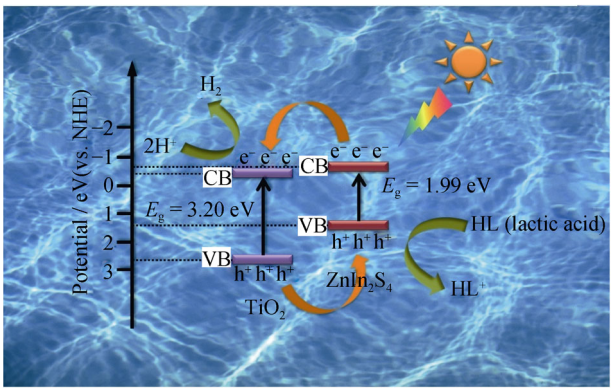

Fig. 6 Schematic illustration of photocatalytic mechanism of H_2 generation process therein

energy, both of them would be excited to generate electron–hole pairs. And the photocatalytic electrons of the $ZnIn_2S_4$ could transfer to TiO_2 via the core–shell interface due to the formation of impacted junction between TiO_2 and $ZnIn_2S_4$, and then, the massive electrons would reduce the protons in the interior cavity to produce hydrogen. Furthermore, the photoinduced holes on the VB of TiO_2 can fast transfer to the VB of $ZnIn_2S_4$, and would be immediately consumed by the sacrificial agent of lattice acid [14, 18–20]. It is emphasized that the core–shell hollow structure would trigger the confinement effect and multiple scattering effect, which could further greatly enhance the HER activity under overall light irradiation [21–36].

4 Conclusion

To sum up, a novel core–shell TiO_2@$ZnIn_2S_4$ hollow nanostructure was successfully designed and synthesized via templating method assisted by hydrothermal synthesis process, and the formed type-II heterojunction in the as-prepared sample could significantly improve the separation and migration of charge carriers. Additionally, the novel core–shell hollow structure could provide suitable interior cavity to trigger the confinement effect and multiple scattering effect, both ultimately resulting in a great photocatalytic H_2 generation of the obtained sample under overall light irradiation.

Acknowledgements This work was financially supported by the National Natural Science Foundation of China (No. U1862105), the Natural Science Basic Research Plan in Shaanxi Province of China (Nos. 2017JZ001 and 2018KJXX-008), the Fundamental Research Funds for the Central Universities (No. cxtd2017004), the Science and Technology Project of Henan Province (No. 182106000029), the Key Research and Development Program of Shaanxi Province (No. 2018ZDCXL-SF-02-04), K. C. Wong Education Foundation, Hong Kong, China and Australian Research Council. We also thank the technical help from International Center for Dielectric Research (ICDR), Xi'an Jiaotong University, Xi'an, China.

References

[1] Wan-Kuen J, Yeon-Ji J. 2D graphene-assisted low-cost metal (Ag, Cu, Fe, or Ni)-doped TiO_2, nanowire architectures for enhanced hydrogen generation. J Alloys Compd. 2018;765:106.
[2] Wah LF, Wei LC, Mun LK, Ching JJ. Enhance of TiO_2 dopants incorporated reduced graphene oxide via RF magnetron sputtering for efficient dye-sensitised solar cells. Rare Met. 2018; 37(11):919.
[3] Li G, Zhao Q, Yang H, Liu Z. Fabrication and characterization of ZnO-coated TiO_2 nanotube arrays. Compos Interface. 2016; 23(2):125.
[4] Li H, Yan X, Lin B, Xia M, Wei J, Yang B, Yang G. Controllable spatial effect acting on photo-induced CdS@CoP@-SiO_2 ball-in-ball nano-photoreactor for enhancing hydrogen evolution. Nano Energy. 2018;47:481.
[5] Lin B, Chen S, Dong F, Yang G. A ball-in-ball g-C_3N_4@SiO_2 nano-photoreactor for highly efficient H_2 generation and NO removal. Nanoscale. 2017;9(16):5273.
[6] Guo P, Shen Y, Song Y, Ma J, Lin YH, Nan CW. Self-etching Ni–Co hydroxides@Ni–Cu nanowire arrays with enhancing ultrahigh areal capacitance for flexible thin-film supercapacitors. Rare Met. 2017;36(9):758.
[7] Wang M, Sun L, Cai J, Huang P, Su Y, Lin C. A facile hydrothermal deposition of $ZnFe_2O_4$ nanoparticles on TiO_2 nanotube arrays for enhanced visible light photocatalytic activity. J Mater Chem A. 2013;1(39):12082.
[8] Xiang Q, Yu J, Jaroniec M. Enhanced photocatalytic H_2-production activity of graphene-modified titania nanosheets. Nanoscale. 2011;3(9):3670.
[9] Yan X, Xue C, Yang B, Yang G. Novel three-dimensionally ordered macroporous Fe^{3+}-doped TiO_2 photocatalysts for H_2 production and degradation applications. Appl Surf Sci. 2017; 394:248.
[10] Zhu Y, Wang L, Liu Y, Shao L, Xia X. In-situ hydrogenation engineering of $ZnIn_2S_4$ for promoted visible-light water splitting. Appl Catal B: Environ. 2019;241:483.
[11] Sun S, Gao L, Liu Y. Enhanced dye-sensitized solar cell using graphene–TiO_2 photoanode prepared by heterogeneous coagulation. Appl Phys Lett. 2010;96(8):083113.
[12] Rangelmendez JR, Matos J, Cházaroruiz LF, González-Castillo AC, Barrios-Yáñez G. Microwave-assisted synthesis of C-doped TiO_2 and ZnO hybrid nanostructured materials as quantum-dots sensitized solar cells. Appl Surf Sci. 2018;434:744.
[13] Motola M, Satrapinskyy L, Čaplovicová M, Roch T, Gregor M, Grančič B, Čaplovič L, Plesch G. Enhanced photocatalytic activity of hydrogenated and vanadium doped TiO_2 nanotube arrays grown by anodization of sputtered Ti layers. Appl Surf Sci. 2018;434:1257.
[14] Lin B, Li H, An H, Hao W, Wei J, Dai Y, Ma C, Yang G. Preparation of 2D/2D g-C_3N_4 nanosheet@$ZnIn_2S_4$ nanoleaf heterojunctions with well-designed high-speed charge transfer nanochannels towards high-efficiency photocatalytic hydrogen evolution. Appl Catal B: Environ. 2017;220:542.
[15] Tian Q, Wu W, Liu J, Wu Z, Yao W, Ding J, Jiang C. Dimensional heterostructures of 1D CdS/2D $ZnIn_2S_4$ composited with 2D graphene: designed synthesis and superior photocatalytic performance. Dalton T. 2017;46(9):2770.
[16] Xue C, Yan X, An H, Li H, Wei J, Yang G. Bonding CdS–Sn_2S_3 eutectic clusters on graphene nanosheets with unusually photoreaction-driven structural reconfiguration effect for excellent

H_2 evolution and Cr(VI) reduction. Appl Catal B: Environ. 2018;222:157.
[17] Chen G, Ning D, Fan LI, Fan Y, Luo Y, Li D, Meng Q. Enhancement of photocatalytic H_2 evolution on $ZnIn_2S_4$ loaded with in situ photo-deposited MoS_2 under visible light irradiation. Appl Catal B: Environ. 2014;160–161:614.
[18] Wei L, Chen Y, Zhao J, Li Z. Preparation of NiS/$ZnIn_2S_4$ as a superior photocatalyst for hydrogen evolution under visible light irradiation. Beilstein J Nanotechnol. 2013;4(12):949.
[19] Li H, Yu H, Chen S, Zhao H, Zhang Y, Quan X. Fabrication of graphene wrapped $ZnIn_2S_4$ microspheres heterojunction with enhanced interfacial contact and its improved photocatalytic performance. Dalton T. 2014;43(7):2888.
[20] Chen Z, Li D, Zhang W, Shao Y, Chen T, Sun M, Fu X. Photocatalytic degradation of dyes by $ZnIn_2S_4$ microspheres under visible light irradiation. J Phys Chem C. 2009;113(11):4433.
[21] Shen S, Chen X, Ren F, Kronawitter CX, Mao SS, Guo L. Solar light-driven photocatalytic hydrogen evolution over $ZnIn_2S_4$ loaded with transition-metal sulfides. Nanoscale Res Lett. 2011; 6(1):290.
[22] Liu Y. Hydrothermal synthesis of TiO_2–RGO composites and their improved photocatalytic activity in visible light. RSC Adv. 2014;4(68):36040.
[23] Xue C, Li H, An H, Yang B, Wei J, Yang G. NiS_x quantum dots accelerate electron transfer in $Cd_{0.8}Zn_{0.2}S$ photocatalytic system via an rGO Nanosheet "Bridge" toward visible-light-driven hydrogen evolution. ACS Catal. 2018;8(2):1532.
[24] Lin B, An H, Yan X, Zhang T, Wei J, Yang G. Fish-scale structured g-C_3N_4, nanosheet with unusual spatial electron transfer property for high-efficiency photocatalytic hydrogen evolution. Appl Catal B: Environ. 2017;210:173.
[25] Chen J, Zhao D, Diao Z, Wang M, Shen S. Ferrites boosting photocatalytic hydrogen evolution over graphitic carbon nitride: a case study of (Co, Ni)Fe_2O_4 modification. Mater Sci. 2016; 61(4):292.
[26] Tan Y, Liu M, Wei D, Tang H, Feng X, Shen S. A single green approach to synthesis of sub-100 nm carbon spheres as template for TiO_2 hollow nanospheres with enhanced photocatalytic activities. Sci China Mater. 2018;61(6):869.
[27] Li Y, Guo Y, Ran L, Dong L, Zhao M, Tan Y, Gao C, Shen S, Xiong Y. Steering plasmonic hot electrons to realize enhanced full-spectrum photocatalytic hydrogen evolution. Chinese J Catal. 2018;39(3):453.
[28] Wang B, Shen S, Mao SS. Black TiO_2 for solar hydrogen conversion. J Mater. 2017;3(2):96.
[29] Shen S, Chen J, Wang M, Sheng X, Chen X, Feng X, Mao SS. Titanium dioxide nanostructures for photoelectrochemical applications. Prog Mater Sci. 2018;98:299.
[30] Wang M, Zhang S, Du ZF, Sun LD, Zhao DL. Novel dye-sensitized solar cell architecture using TiO_2-coated Ag nanowires array as photoanode. Chin J Rare Met. 2019;38(4):316.
[31] Low FW, Lai CW, Hamid SBA. Surface modification of reduced graphene oxide film by Ti ion implantation technique for high dye-sensitized solar cells performance. Ceram Int. 2017;43(1): 625.
[32] Zhai YQ, Li RF, Li X, Li JH. Rapid synthesis and properties of color-tunable phosphors $SrMoO_4$: Eu^{3+}, Tb^{3+}. Rare Met. 2017; 36(10):828.
[33] Sun K, Fan RH, Zhang ZD, Yan KL, Zhang XH, Cheng CB, Chen M, Xie PT. Electromagnetic attenuation property of multiphase Fe–Fe_3O_4–Al_2O_3 cermets near percolation threshold. Rare Met. 2017;36(1):42.
[34] You JH, Wang RC, Han F, Guo R, Liu XW. Synthesis and luminescence properties of Mn^{3+}, Bi^{3+} co-doped Y_6WO_{12} for blue phosphor. Rare Met. 2018;37(5):439.
[35] Yan YC, Shi W, Jiang HC, Xiong J, Zhang WL. Fabrication and characterization of NiO films for energetic nano-multilayers by direct current reactive sputtering. Rare Met. 2018;37(7):594.
[36] Wachiraporn M, Anukorn P, Somchai T, Titipun T. Photoluminescence and photonic absorbance of $Ce_2(MoO_4)_3$ nanocrystal synthesized by microwave hydrothermal solvothermal method. Rare Met. 2018;37(10):868.